FDTD modeling of solar energy absorption in silicon branched nanowires

Christin Lundgren[1], Rene Lopez[2], Joan Redwing[3], and Kathleen Melde[1,*]

[1]*Department Electrical and Computer Engineering, University of Arizona, E. Speedway Blvd., Tucson, AZ, 85721, USA*

[2]*Department Physics and Astronomy, University of North Carolina, Chapel Hill, NC, 27599, USA*

[3]*Department Materials Science and Engineering, Pennsylvania State University, University Park, PA 16802, USA*

[*]*melde@email.arizona.edu*

Abstract: Thin film nanostructured photovoltaic cells are increasing in efficiency and decreasing the cost of solar energy. FDTD modeling of branched nanowire 'forests' are shown to have improved optical absorption in the visible and near-IR spectra over nanowire arrays alone, with a factor of 5 enhancement available at 1000 nm. Alternate BNW tree configurations are presented, achieving a maximum absorption of over 95% at 500 nm.

OCIS codes: (000.3860) Mathematical methods in physics; (000.4430) Numerical approximation and analysis; (350.6050) Solar energy.

References and links

1. T. M. Razykov, C. S. Ferekides, D. Morel, E. Stefanakos, H. S. Ullal, and H. M. Upadhyaya, "Solar photovoltaic electricity: Current status and future prospects," Sol. Energy **85**(8), 1580–1608 (2011).
2. B. M. Kayes, H. A. Atwater, and N. S. Lewis, "Comparison of the device physics principles of planar and radial p-n junction nanorod solar cells," J. Appl. Phys. **97**(11), 114302 (2005).
3. E. Garnett and P. Yang, "Light Trapping in Silicon Nanowire Solar Cells," Nano Lett. **10**(3), 1082–1087 (2010).
4. E. Barraud, "New world record efficiency for thin film silicon solar cells," *http://actu.epfl.ch/news/new-* world-record-efficiency-for-thin-film-silicon-/
5. M. D. Kelzenberg, S. W. Boettcher, J. A. Petykiewicz, D. B. Turner-Evans, M. C. Putnam, E. L. Warren, J. M. Spurgeon, R. M. Briggs, N. S. Lewis, and H. A. Atwater, "Enhanced absorption and carrier collection in Si wire arrays for photovoltaic applications," Nat. Mater. **9**(3), 239–244 (2010).
6. M. J. Bierman and S. Jin, "Potential applications of hierarchical branching nanowires in solar energy conversion," Energy Environ. Sci. **2**(10), 1050–1059 (2009).
7. C. Cheng and H. J. Fan, "Branched nanowires: Synthesis and energy applications," Nano Today **7**(4), 327–343 (2012).
8. D. Wang, F. Qian, C. Yang, Z. H. Zhong, and C. M. Lieber, "Rational Growth of Branched and Hyperbranched Nanowire Structures," Nano Lett. **4**(5), 871–874 (2004).
9. K. A. Dick, K. Deppert, M. W. Larsson, T. Mårtensson, W. Seifert, L. R. Wallenberg, and L. Samuelson, "Synthesis of branched 'nanotrees' by controlled seeding of multiple branching events," Nat. Mater. **3**(6), 380–384 (2004).
10. C. Yan, X. P. Li, K. Zhou, A. Pan, P. Werner, S. L. Mensah, A. T. Vogel, and V. Schmidt, "Heteroepitaxial growth of GaSb nanotrees with an ultra-low reflectivity in a broad spectral range," Nano Lett. **12**(4), 1799–1805 (2012).
11. K. Sun, Y. Jing, C. Li, X. F. Zhang, R. Aguinaldo, A. Kargar, K. Madsen, K. Banu, Y. C. Zhou, Y. Bando, Z. W. Liu, and D. Wang, "3D branched nanowire heterojunction photoelectrodes for high-efficiency solar water splitting and H2 generation," Nanoscale **4**(5), 1515–1521 (2012).
12. Y. J. Hwang, C. H. Wu, C. Hahn, H. E. Jeong, and P. D. Yang, "Si/InGaN core/shell hierarchical nanowire arrays and their photoelectrochemical properties," Nano Lett. **12**(3), 1678–1682 (2012).
13. H. P. Yoon, Y. A. Yuwen, C. E. Kendrick, G. D. Barber, N. J. Podraza, J. M. Redwing, T. E. Mallouk, C. R. Wronski, and T. S. Mayer, "Enhanced conversion efficiencies for pillar array solar cells fabricated from crystalline silicon with short minority carrier diffusion lengths," Appl. Phys. Lett. **96**(21), 213503 (2010).
14. A. F. Oskooi, D. Roundy, M. Ibanescu, P. Bermel, J. D. Joannopoulos, and S. G. Johnson, "Meep: A flexible free-software package for electromagnetic simulations by the FDTD method," Comput. Phys. Commun. **181**(3), 687–702 (2010).
15. A. Taflove and S. C. Hagness, *Computational Electrodynamics: The Finite-Difference Time-Domain Method, Third Edition*, 3rd ed. (Artech House, 2005).
16. S. Q. Li, P. Guo, L. Zhang, W. Zhou, T. W. Odom, T. Seideman, J. B. Ketterson, and R. P. H. Chang, "Infrared Plasmonics with Indium-Tin-Oxide Nanorod Arrays," ACS Nano **5**(11), 9161–9170 (2011).
17. A. Deinega and S. John, "Effective optical response of silicon to sunlight in the finite-difference time-domain method," Opt. Lett. **37**(1), 112–114 (2012).

#182328 - $15.00 USD Received 27 Dec 2012; revised 1 Apr 2013; accepted 2 Apr 2013; published 9 Apr 2013

18. S. G. Johnson, "Materials in Meep," http://ab-initio.mit.edu/wiki/index.php/Material_dispersion_in_Meep.
19. M. A. Green, "Self-consistent optical parameters of intrinsic silicon at 300 K including temperature coefficients," Sol. Energy Mater. Sol. Cells **92**(11), 1305–1310 (2008).
20. L. Hu and G. Chen, "Analysis of Optical Absorption in Silicon Nanowire Arrays for Photovoltaic Applications," Nano Lett. **7**(11), 3249–3252 (2007).
21. K.-T. Park, Z. Guo, H.-D. Um, J.-Y. Jung, J. M. Yang, S. K. Lim, Y. S. Kim, and J.-H. Lee, "Optical properties of Si microwires combined with nanoneedles for flexible thin film photovoltaics," Opt. Express **19**(S1 Suppl 1), A41–A50 (2011).
22. M. M. Braun and L. Pilon, "Effective optical properties of non-absorbing nanoporous thin films," Thin Solid Films **496**(2), 505–514 (2006).
23. P. Han, Y. W. Chen, and X.-C. Zhang, "Application of Silicon Micropyramid Structures for Antireflection of Terahertz Waves," IEEE J. Sel. Top. Quantum Electron. **16**(1), 338–343 (2010).
24. J. D. Joannopoulos, S. G. Johnson, J. N. Winn, and R. D. Meade, *Photonic Crystals: Molding the Flow of Light*, 2nd ed. (Princeton University Press, 2008).
25. J. Zhu, Z. Yu, G. F. Burkhard, C.-M. Hsu, S. T. Connor, Y. Xu, Q. Wang, M. McGehee, S. Fan, and Y. Cui, "Optical Absorption Enhancement in Amorphous Silicon Nanowire and Nanocone Arrays," Nano Lett. **9**(1), 279–282 (2009).

1. Introduction

Affordable solar power is an attractive prospect for a number of reasons, including the declining availability of nonrenewable fossil fuels. In order to make solar energy viable on a large scale, the efficiency of photovoltaic cells must increase or the cost of production and materials must decrease below the current $1.50 per Watt of polycrystalline silicon PV cells [1]. Thin film photovoltaic cells demonstrate the prospects of increasing efficiency and decreasing material costs [2, 3]. In February 2013, the best single junction Si thin film solar cell achieved 10.7% efficiency [4]. In contrast, new research in solar cells using nanowire structures have a proven efficiency of 8.40% and branched nanowire devices may exceed that, based on increased optical absorption [5–7]. Research in nanowire (NW) and branched nanowire (BNW) Si solar cells is still relatively new compared to thin film bulk solar cells.

Besides cell efficiency, there are differences between the materials and processing of planar and nanowire solar cells. In planar Si devices, as shown in Fig. 1(a), high purity single-crystal Si is required in order to maximize absorption of the incident solar radiation and achieve sufficiently long minority carrier diffusion lengths. Planar cells that use (less expensive) materials with a higher level of impurities and crystalline defects typically leads to a reduction in the minority carrier diffusion length and thus reduced cell efficiency. The p-n junctions in the nanowire arrays are radial, as shown in Fig. 1(b), with very short diffusion distances. This configuration allows the use of less expensive materials with higher level of impurities and crystalline defects. Si NW arrays occupy a fraction of the array volume with wafer based devices and have shown to exceed the ray-optics light-trapping absorption limit of an equivalent volume of textured planar Si. Si nanowire cells show a broadband, near unity internal quantum efficiency for carrier generation because of relatively short diffusion lengths for the minority carriers [2]. Maximizing efficiency requires that the wire array provide high absorption and be sized for efficient carrier collection.

Prior studies of branched nanowires primarily focused on experimental investigations of nanowire synthesis and characterization of the structural and optical properties of the resulting nanostructured surfaces. This work has been the topic of several recent review articles [5, 6]. Branched nanowire synthesis builds on the prior work utilizing bottom-up growth techniques such as vapor-liquid-solid (VLS) or solution-liquid-solid (SLS) growth for the fabrication of vertical nanowire arrays. The initial nanowire "trunks" serve as the substrate

#182328 - $15.00 USD Received 27 Dec 2012; revised 1 Apr 2013; accepted 2 Apr 2013; published 9 Apr 2013

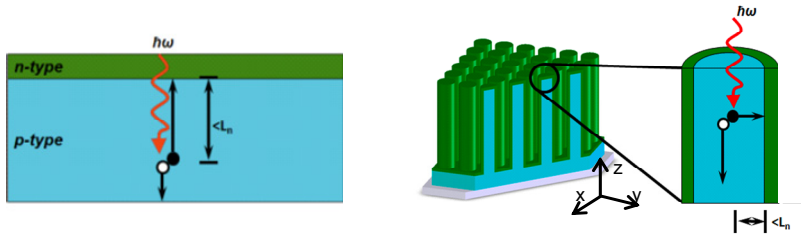

Fig. 1. Light and carrier interactions in Si junctions (a) planar junction, (b) radial junction.

for the subsequent epitaxial growth of branches. Branched nanowire structures have been demonstrated in a variety of semiconductor materials systems such as Si [8], GaP [9] and GaSb [10] as well as oxides such as ZnO, SnO2 and TiO2 [7]. Branching provides an additional pathway to enhance device performance through the fabrication of branched nanowire heterostructures. For example, nanostructured surfaces consisting of ZnO NW [11] and InGaN NW [12] branches formed on Si NW trunks have been investigated for use as photoelectrochemical cells for solar water splitting.

The branched nanowire arrays described in this paper have the potential to increase the optical absorption while simultaneously decreasing the carrier diffusion length of the photovoltaic device [13]. The aim of this paper is to model a branched nanowire structure with enhanced light absorption, and to present an understanding of the photonic and electromagnetic characteristics of the tree and the forest array geometry.

2. Modeling

2.1 Procedure

Meep, a finite-difference time-domain (FDTD) 3-dimensional electromagnetic field simulation package, was used to model the BNW arrays [14]. FDTD is a good choice to model a wide bandwidth, since it uses a time-domain pulse made up of multiple frequencies [15]. Additionally, Meep is a robust open-source package that has been used in modeling nanostructures for other applications [16].

It is possible to obtain good results for optical reflection using only a single frequency-independent value for the real part of the material dielectric constant. However, modeling absorption requires the use of the imaginary part of the dielectric constant as well. A physically-consistent complex dielectric constant expressed as a continually varying function of frequency is the ideal, but it is not a practical solution for FDTD computations, where each input pulse is the sum of multiple frequency components. One way Meep handles complex dielectric materials is with a Lorentzian dielectric model. Unfortunately, it is difficult to represent the dielectric constant of silicon as a Lorentzian with a reasonable number of terms over a wide band that encompasses the visible and near-IR spectra [17]. This computational method was rejected because accurate dielectric characteristics are needed over a wide bandwidth of 500 nm.

A second way that Meep incorporates a complex dielectric material is by integrating the conductivity, σ_D, into the form of Maxwell's equation used by the solver. The equation for the electric field, $\vec{D} = \varepsilon \bullet \vec{E}$, is extended to include the polarization term, P, and P is a frequency-dependent function of the real and imaginary parts of the dielectric constant. To use this feature, set the conductivity σ_D, such that $\varepsilon'' = 2\pi \bullet f \bullet \varepsilon_r$ [18].

To make the simulation physically realistic, and account for the fact that n and k both change significantly in the higher frequency end of the band in question, a stitching technique is used to compensate. The entire model geometry simulation is performed at several center frequencies, each with a narrow band. The dielectric parameters used are n and k, the real and

#182328 - $15.00 USD Received 27 Dec 2012; revised 1 Apr 2013; accepted 2 Apr 2013; published 9 Apr 2013

imaginary parts of the index of refraction from [19]. The output results are stitched together using an m-dimensional Bezier curve, where m is the total number of points. This provides a good approximation of the continually varying dielectric properties of the material.

Since Meep sources have arbitrary values, the resulting EM fields are proportional to the input but have no fixed value. Thus, constant illumination with respect to frequency was used to facilitate comparison between simulation runs.

To verify the effectiveness of this modeling technique, an array of silicon nanowires was simulated and compared to results from the literature as was done in [3]. Nanowires with radius r = 25 nm, length L = 2.33 μm, and lattice spacing a = 100 nm were modeled and were found to be closely matched to the comparable results of the transfer matrix method (TMM) presented in [20] (Fig. 2). The wavelength sweep in this case was chosen to coincide with the results presented in [20].

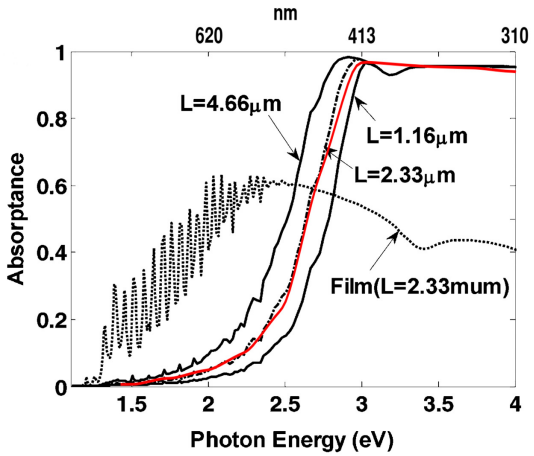

Fig. 2. Simulation of NW array with r = 25 nm, L = 2.33 μm, and a = 100 nm (orange) compared with TMM results from [20].

2.2 Branched nanowire parameter study

Once the first simulation procedure was created and verified through comparison, it was used to model a forest comprising silicon trees to demonstrate the computational value of the FDTD modeling technique in Meep. Figure 3 shows the geometry of the branched nanowire structures. Figure 4 shows the reference solar spectrum used for the BNW simulations for the parameter study. The simulations were run for the 0.5 to 1 μm (500 to 1000 nm) wavelength range since this is the range has the highest values of irradiance and can be used to generally assess the bulk optical characteristics of the BNW forest. The power absorbed by the BNW forest is determined by multiplying the percentage of energy absorbed by the irradiance values of Fig. 4 for the corresponding wavelength.

Figure 5 shows the results for a BNW array with branch spacing s = 0.7 μm and 2.5 μm. Trunk heights represented are h = 5, 10, 15, 20, and 25 μm. The BNW forest is less sensitive to the lattice spacing than a comparable NW array. Increasing the height of the trees increases the optical absorption, but only up to a point, occurring at roughly h = 20 μm.

#182328 - $15.00 USD Received 27 Dec 2012; revised 1 Apr 2013; accepted 2 Apr 2013; published 9 Apr 2013

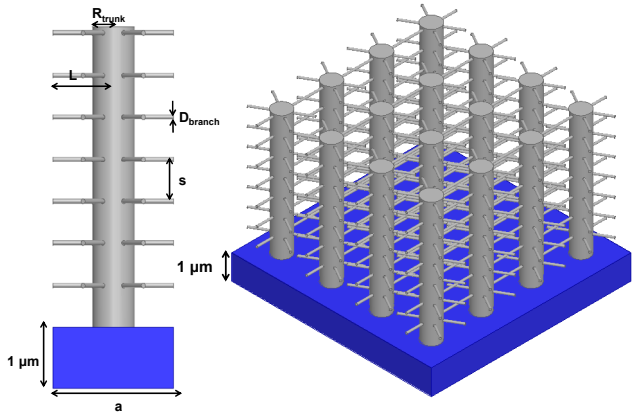

(a) (b)

Fig. 3. (a) Dimensions of a single branched nanowire tree. (b) Array of BNW trees.

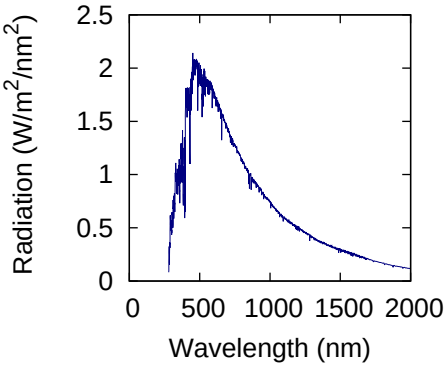

Fig. 4. Reference solar spectrum for Si BNW simulations.

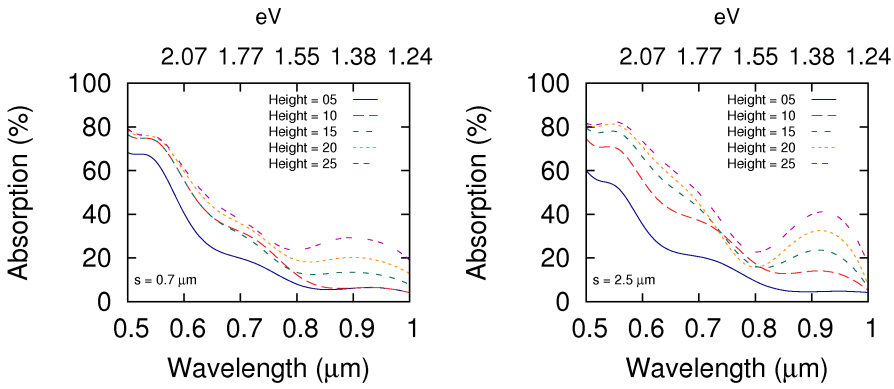

(a) (b)

Fig. 5. BNW forest with R_{trunk} = 0.35 μm, lattice spacing a = 2 μm, height h = 10 μm, branch radius R_{branch} = 0.04. Height ranges from 5 – 25μm. (a) Branch spacing s = 0.7 μm. (b) Branch spacing s = 2.5 μm.

The optical absorption for a wide range of parameters is depicted in Fig. 6. Figures 6(c) and 6(d) demonstrate that the optical absorption of the BNW forest is enhanced over that of a

#182328 - $15.00 USD Received 27 Dec 2012; revised 1 Apr 2013; accepted 2 Apr 2013; published 9 Apr 2013

plain NW array with the same dimensions. The performance at the low end of the band (0.5 μm) is very similar, but there is an increase of at least 4 times at a wavelength of 1 μm.

Increasing the radius, R_{trunk} of the main trunk has a relatively minor effect on the absorption and reflection of the system. The array lattice spacing *a* also has a small effect on the optical properties of the structure, unlike in a nanowire array where the optical properties have a strong dependence on *a*.

If the branches remain the same length *L*, and that length is less than *a*, then increasing *a* has the effect of decreasing optical absorption. If the length of the branches is increased proportionally with *a*, however, the additional space between the individual trunks is filled with branches, so the net result is similar absorption and reflection results.

An analogy can be made with microwave engineering, where antennas are also arranged in arrays. Sub-wavelength spacing is employed to increase directivity and spacing greater than a wavelength is used to obtain isotropic gain. A smaller spacing between branches may be able to take advantage of the photonic crystalline nature of the BNW forest structure.

3. Physical characteristics

3.1 Overall dielectric properties

As the lattice spacing decreases and the branch length and radius of the BNW increase, there is a corresponding increase in the total surface area of the silicon in the forest. This has the potential to increase absorption of incident energy. However, as the density increases, the surface plane of the forest appears to approach a porous material with effective bulk dielectric characteristics. It is worth considering whether the improvement in absorption and reflection properties of the thin film BNW are simply a result of an effective permittivity less than that of silicon providing a transition layer to the substrate.

One way to explore this is to compare the BNW reflection and transmission results with those of a nanowire array with the same feature sizes. Figures 6(c) and 6(d) show that all of the BNW forest configurations except for the case with the narrowest branches have higher absorption than the nanowires alone.

Another method of comparison is with the mathematical computation of the appropriate effective dielectric constant value applied to the calculation of reflectance and transmittance using classical electromagnetic theory. Volume averaging theory (VAT) is a technique which can be used to calculate the effective dielectric constant of a nanoporous material Eq. (1).

VAT is valid for TE modes and acceptable for TM modes for nanostructured materials with an a/b feature aspect ratio greater than 1, and good for both modes with a/b > 2, where *a* is the vertical spacing between dielectric features, and *b* is the horizontal spacing between feature. In the referenced paper, the nanoscale features are pores; *a* = vertical spacing, *b* = horizontal spacing. Overall, VAT is applicable to structures with horizontal layers, such as the BNW [21].

$$\eta_{eff} = (1-\phi)\eta_c + \phi\eta_d \tag{1}$$

$$\mathrm{R} = \mathrm{R_P} = \mathrm{R_\perp} = \left(\frac{\eta_d - \eta_i}{\eta_d + \eta_i}\right)^2 \tag{2}$$

$$\mathrm{T} = \mathrm{T_P} = \mathrm{T_\perp} = \frac{4\eta_d\eta_i}{(\eta_d + \eta_i)^2} \tag{3}$$

The effective index of refraction was calculated using Eq. (1). ϕ is the porosity, n_c is the real index of refraction of the continuous phase material, silicon, and n_d is the real index of refraction of the dispersed phase material, air.

With R_{trunk} = 0.35 and R_{branch} = 0.25, the volume fill factor of silicon in the layer of branches at the surface interface is 77%, so ϕ is 0.33, n_{eff} is 3.09.

#182328 - $15.00 USD Received 27 Dec 2012; revised 1 Apr 2013; accepted 2 Apr 2013; published 9 Apr 2013

Using the Fresnel reflection equation at normal incidence Eq. (2), the calculated expected value of reflection is 26%. The VAT is used with Maxwell's equations. We can assume that using the classical Fresnel equations are acceptable since they derive from Maxwell's equations at a dielectric boundary. Equation (2) is the reflectance and Eq. (3) is the transmittance of normally incident light at a dielectric interface. Note that since the VAT uses the real indices of refraction, only the reflectance can be compared with the Meep results, which incorporate the complex indices of refraction.

With a lower surface fill factor of 25%, n_{eff} is 1.61 and the calculated reflection is decreased to 6%, but less area is available to absorb the incident light. The branches, like microwires, can be considered a contributor to a lower effective index of refraction, improving reflection of incident light [22]. It is apparent from the results presented in Table 1 that the presence and size of the nanowires and branches have a strong role in guiding the incident light into the forest to be absorbed effectively, and that the optical properties of the thin film are not solely a result of the bulk dielectric material characteristics.

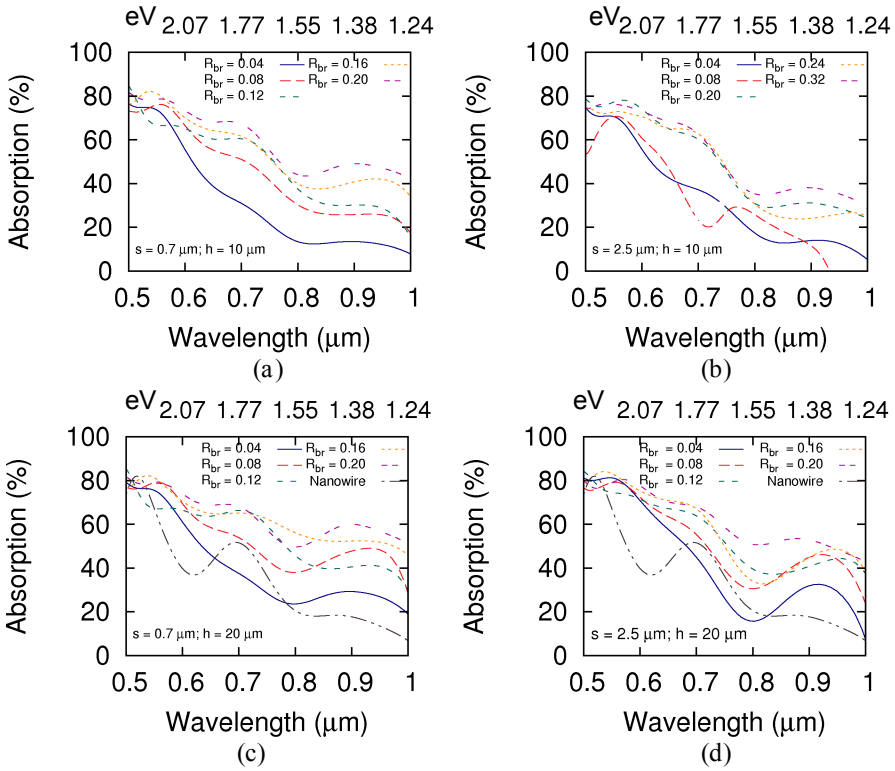

Fig. 6. BNW forest with R_{trunk} = 0.35 μm, a = 2 μm. (a) Branch spacing s = 0.7 μm, trunk height h = 10 μm, branch radius R_{branch} = 0.04 – 0.28 μm. (b) s = 2.5 μm, h = 10 μm, R_{branch} = 0.04 – 0.32 μm. (c) s = 0.7 μm, h = 20 μm, R_{branch} = 0.04 μm; compared to NW with a = 2 μm, h = 20 μm. (d) s = 2.5 μm, h = 10 μm, R_{branch} = 0.04 – 0.28 μm. s = 2.5 μm, h = 20 μm, R_{branch} = 0.04 – 0.20 μm; compared to NW with a = 2 μm, h = 20 μm.

#182328 - $15.00 USD Received 27 Dec 2012; revised 1 Apr 2013; accepted 2 Apr 2013; published 9 Apr 2013

Table 1. Reflectance and transmittance for branched nanowires with R_{trunk} = 0.35 μm, a = 1 μm. s = 0.7 μm, L = 0.5 μm, trunk height h = 20 μm, branch radius R_{branch} = 0.25 μm.

Wavelength (nm)	n_d	n_{eff}	Meep Results for BNW		VAT Results for BNW		Meep Results for NW only	
			R	T	R	T	R	T
500	4.29	3.53	21.1%	0%	31.2%	68.9%	21.1%	40.6%
750	3.72	3.09	28.6%	0%	26.1%	73.9%	11.1%	10.4%
1000	3.57	2.98	23.3%	7.4%	24.8%	75.2%	16.3%	61.0%

3.2 Photonic crystalline properties

The BNW structure can be considered a 3-dimensional photonic crystal (PC). It has a repeating geometry in three directions which affects the propagation of light through the forest region. The intended use of this structure is different from the standard PC, whose desired behavior in a given frequency band is either a complete bandgap, reflecting the incident light, or a passband, commonly used in anti-reflection coatings and wave guiding [23, 24].

This forest of silicon is a hybrid of these two purposes. It should guide the incident energy into the forest region and then re-reflect and disperse the light to be absorbed by the trees as effectively as possible.

This leads naturally into thinking about other forest configurations that either suppresses cavity resonances or that do not have large ε_{eff} at the surface plane.

4. Design

4.1 Alternate forest configurations

Several different forest configurations are to be simulated, to investigate the possibility of increasing the array absorption efficiency. Treating the forest as a photonic crystal provides some insight into the likely behavior of a forest comprising each type of tree.

The trees under consideration are as follows (Fig. 7, left):

- Scrub: branches only on the lower half of the trunk. This may allow reflection from branches to be absorbed into the upper half of the trunk instead of being reflected away from the device.
- Canopy: branches only on the upper half of the trunk. This may cause more reflection, but it may also allow reflection from substrate to be reabsorbed by the bottom layer of branches.
- Conifer: branches of graduated length- long at the substrate, none at the tip. This is a more nuanced implementation of the scrub forest. It may allow back reflections many chances to be reabsorbed through multiple layers of branches.

The results of the various BNW forest designs are shown in the plot in Fig. 7 (right side). It is clear that the conical conifer forest structure has the clear advantage in optical absorption. A low effective index of refraction at the device's surface combined with the broadband enhancements typical of a conical or angled feature shape (such as nanocones vs. nanocylinders) create significant absorption throughout the entire wavelength band, with a maximum absorption of 97% at 0.5 μm, and nearly 70% at 1 μm [25].

#182328 - $15.00 USD Received 27 Dec 2012; revised 1 Apr 2013; accepted 2 Apr 2013; published 9 Apr 2013

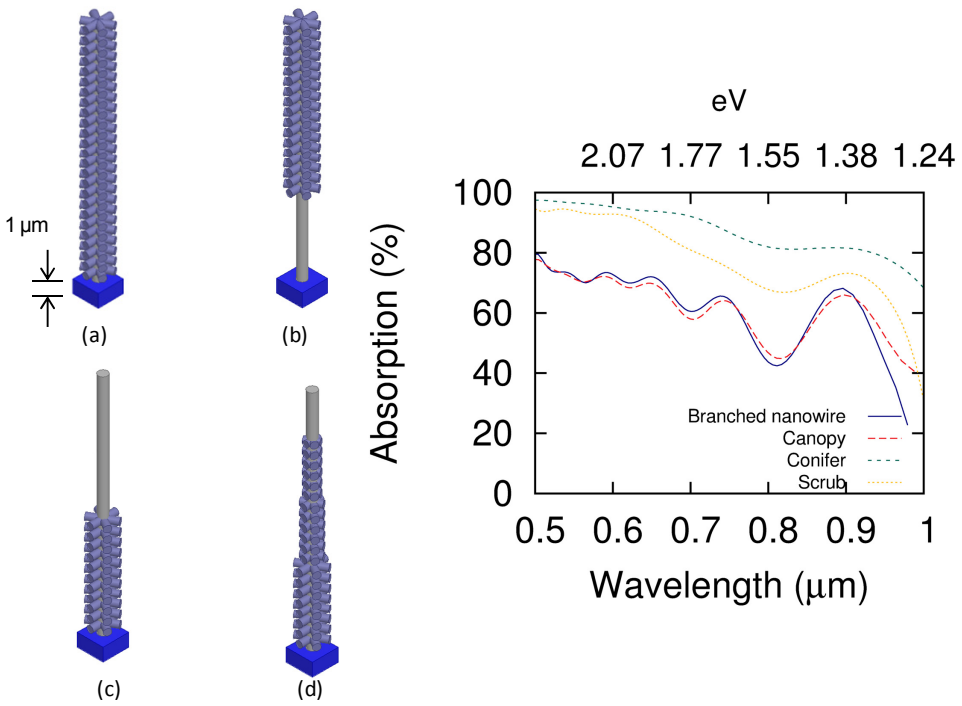

Fig. 7. [Left side] BNW forest configurations. (a) Plain BNW tree; (b) Canopy; (c) Scrub; (d) Conifer. [Right side] Results for BNW tree, canopy, conifer, and scrub forest arrays for R_{trunk} = 0.35 µm, a = 2 µm, branch spacing s = 0.7 µm, trunk height h = 20 µm, branch radius R_{branch} = 0.25 µm, branch length L = 5

The scrub forest is an improvement over the BNW forest, with some of the light that is reflected from the surface of the interlocking branches absorbed by the trunks instead of being reflected. The canopy structure has very similar optical characteristics to the BNW, due mainly to reflection effects at the surface of the array.

The overlapping of the long (L = 5 µm) branches contributes to the local maximum in the BNW absorption at 0.9 µm.

5. Conclusion

Computational modeling using the Meep FDTD simulation package demonstrates that branched nanowire arrays have significant enhancements over nanowire array structures, with at least a factor of 4 improvement available in the difficult low energy region near 1 µm.

Alternate BNW array design simulations are presented. The conical BNW canopy forest achieves a 97% absorption for a 0.5 µm wavelength.

Acknowledgments

This work was supported in part by the Research Corporation for Scientific Advancement: Scialog Collaborative Innovation Award (No. 20283) and by the National Science Foundation under Grant ECCS-1231368.

#182328 - $15.00 USD Received 27 Dec 2012; revised 1 Apr 2013; accepted 2 Apr 2013; published 9 Apr 2013